Maximizing exchange–bias in Co/CoO core/shell nanoparticles by lattice matching between the shell and the embedding matrix.

Juan A. González[*], Juan P. Andrés, Ricardo López Antón, José A. De Toro, Peter S. Normile, Pablo Muñiz, J. Manuel Riveiro and Josep Nogués[†,‡].

Instituto Regional de Investigación Científica Aplicada (IRICA) and Dto. de Física Aplicada, Universidad de Castilla–La Mancha, 13071 Ciudad Real, Spain

[†] Catalan Institute of Nanoscience and Nanotechnology (ICN2), CSIC and The Barcelona Institute of Science and Technology, Campus UAB, Bellaterra, 08193 Barcelona, Spain

[‡] ICREA, Pg. Lluís Companys 23, 08010 Barcelona, Spain

ABSTRACT: The exchange bias properties of 5 nm Co/CoO ferromagnetic/antiferromagnetic core/shell nanoparticles, highly dispersed in a Cu_xO matrix, have been optimized by matching the lattice parameter of the matrix with that of the CoO shell. Exchange bias and coercivity fields as large as H_E = 7780 Oe and H_C = 6950 Oe are linked to the presence of a Cu_2O matrix (0.3% lattice mismatch with respect to the shells). The small mismatch between Cu_2O and CoO plays a dual role, (i) structurally stabilizing the CoO and (ii) favoring the existence of a large amount of uncompensated moments in the shell that enhance the exchange bias effects. The results evidence that lattice matching may be a very efficient way to improve the exchange bias properties of core/shell nanoparticles, paving the way to novel approaches to tune their magnetic properties.

INTRODUCTION

Exchange bias refers to a set of different phenomena (e.g., loop shifts in the field axis, H_E, coercivity enhancement or loop asymmetries, among others) which arise when two materials with significantly different magnetic anisotropy, typically a ferromagnet (FM) and an antiferromagnet (AFM), are exchanged coupled at their mutual interface.[1–5] Although most devices exploiting exchange bias effects rely on thin films,[6–8] new applications based on nanoparticles, such as coercivity enhancement for permanent magnets[9,10], microwave absorbers[11] or novel spintronic devices,[12,13] are continuously emerging. Driven by the existing and prospective applications, there is currently a trend to try to enhance the different exchange bias–related effects.[1,2,4,5] In this respect, although archetypical exchange bias systems, e.g., AFM/FM bilayers or FM–AFM core/shell nanoparticles, typically exhibit H_E values in the range of tens to hundreds of Oe;[1,2,4,5] H_E values in excess of 10 kOe have also been occasionally reported.[14–19] However, apart from some possible minor–loop issues,[20,21] many of these systems are based on phase–separation.[14,16,17] This leads to ill–defined FM and AFM counterparts often with FM phases of very small dimensions. Another strategy to obtain very large values for H_E is using FM materials with very low magnetization.[15,18] H_E has been classically expressed as $\mu_0 H_E M_{FM} V = \gamma A$, where M_{FM} is the FM magnetization, V is the volume of the ferromagnet, γ is the interfacial coupling energy per unit surface area, and A is the associated surface area (leading to the well–known expression $\mu_0 H_E = \gamma / M_{FM} t_{FM}$ for thin films).[2] Thus, reducing M_{FM} and t_{FM} are two obvious approaches to enhance H_E. From the applied viewpoint, however, these may be rather unpractical due to the reduced magnetic moment. Improving H_E using γ may be more appealing, despite being more challenging since γ is still not well understood. Although to a first approximation γ should only depend on the intrinsic properties of the FM and AFM materials and their mutual

exchange interactions, many other parameters have been shown to affect γ (e.g., defects, crystalline orientation, crystallinity, thickness of the AFM, roughness or AFM domains).[2,22–26] It has been also shown that the presence of defects and/or impurities in the AFM component, even far from the FM/AFM interface, can dramatically affect the amount of exchange bias.[27–29] While considerable effort has been devoted in thin film systems to harness the diverse mechanisms affecting H_E,[2,4] the role of these effects in core/shell nanoparticles has been far less investigated.[1,3,5]

Due to its appealing properties (e.g., a large interface energy, γ) one of the most studied FM/AFM core/shell systems is Co/CoO.[30–42] Interestingly, in this system H_E values ranging from a few to thousands of Oe have been reported for relatively similar nanoparticles. Several effects have been reported to influence H_E in Co/CoO: core diameter,[34,39,40] shell thickness,[34,37,39,40] crystallinity of the shell,[32,43,44] exchange interactions with neighboring particles,[32,45] strains,[34] orbital moments,[45] uncompensated spins[33,41] and the matrix they are embedded in (through lattice matching effects or antiferromagnetic proximity effects).[31,33,36,46] Concerning the role of the matrix in Co/CoO, H_E values extending from 10 Oe (in non–AFM – non–lattice matched matrices, e.g., Al_2O_3)[31] to 7500 Oe (in AFM – lattice matched matrices, e.g., CoO)[31,36] have been reported for rather similar nanoparticles. Despite this rather large spread of experimental H_E values, there is a lack of systematic studies aimed at elucidating the role of the embedding matrix in the improvement of the exchange bias related properties in core/shell nanoparticles, i.e., at maximization of the effect.

Here we present a systematic study of the magnetic properties of Co/CoO core/shell clusters deposited in a Cu_xO matrix under different oxygen partial pressures, p_{O2}. The magnetic properties are optimized for oxygen pressures yielding matri-

ces with a majority Cu_2O component, which provides an almost perfect lattice matching with the CoO shell. The results indicate that the lattice matching induces a structural stabilization (i.e., improved crystallinity) of the CoO and the concomitant migration of Cu atoms into the shell, enhancing the density of AFM uncompensated spins vital for large H_E field relatively high exchange bias blocking temperature.

EXPERIMENTAL

The samples have been grown by a combination of a vapor phase aggregation technique (i.e., a cluster source) and conventional sputtering.[47] Pure Co nanoparticles are pre–formed in the cluster source by sputtering in an Ar+He atmosphere of about 0.1 mbar.[47] These are then injected by differential pumping into the sputtering deposition chamber where the Ar pressure is two orders of magnitude lower. Importantly, in the main chamber a controlled amount of O_2 is also present (with partial pressures $p_{O2} = 0$ to $5 \cdot 10^{-4}$ mbar). The nanoparticles are thus partially oxidized during their flight towards the substrate, forming a core/shell structure with a Co core and a CoO shell. A Cu target is simultaneously sputtered as the particles arrive at the substrate.[47] This leads to the Co/CoO nanoparticles being embedded in a Cu_xO matrix (where the precise crystallographic composition of the matrix depends on the O_2 partial pressure). The deposition rates of particles and matrix were adjusted to guarantee a high dilution degree of nanoparticles (less than 1 % by volume). Finally the oxygen gas was removed and a capping layer of pure Nb was deposited in order to prevent further (ex–situ) oxidation.[48]

Transmission electron microscopy (TEM) using a FEI Tecnai G2 F20 TEM operated at 200 kV was performed on nanoparticles deposited on a TEM–grid in the absence of oxygen and without a matrix or capping layer.

X–ray diffraction was carried out using a laboratory source (CuK$_\alpha$ radiation) and Bragg–Brentano geometry. Diffraction patterns were analyzed using the Rietveld method implemented via FullProf.[49]
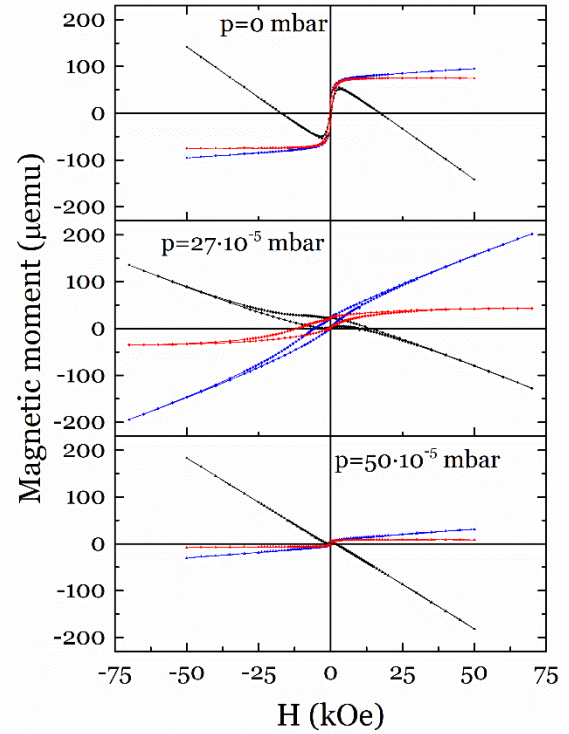

Figure 1. Hysteresis loops (with different corrections) of samples grown in $p_{(O2)}=0$, 27 and 50 $\cdot 10^{-5}$ mbar, at 10K, after cooling from 330K in a saturating field. Black: as measured, blue: after removing substrate contribution; red: after removing the remaining high field susceptibility.

Magnetic properties were measured in a SQUID magnetometer. Hysteresis loops were obtained at fixed temperatures between 10K and 330K after field cooling from 330 K to 10 K using an applied field $H_{FC} = 5o$ kOe. Note that depending on the coercivity (H_C) of the sample, a maximum field of either 50 kOe or 70 kOe was used to avoid minor loop effects.[20,21] The as–obtained hysteresis loops present a negative slope at high fields (Fig. 1, black symbols). To separate the contribution of the substrate from that of the composite films, the high field susceptibility of the substrates was carefully evaluated and subtracted from the data (Fig. 1, blue symbols). The resulting loops then show a positive slope, originating from the films. Finally, to obtain the exchange bias parameters (H_E, H_C and vertical shift)[50] the high field slope, χ_{HF}, was also subtracted (Fig. 1, red symbols).

RESULTS AND DISCUSSION

Fig. 2 shows a TEM image of the nanoparticles together with the corresponding particle size histogram. As can be seen the size distribution is rather narrow with more than one third of the particles with sizes between 4.5 and 5 nm. An independent estimation of the size can be obtained from the superparamagnetic behavior of the nanoparticles at high temperatures. The fit of the room temperature hysteresis loop of the sample with $p_{O2} = 0$ to a Langevin function[51] yields an average nanoparticle moment of (10200 ± 200) μ_B (see inset of Fig. 3), which translates to an average nanoparticle diameter of (5.01 ± 0.03) nm (assuming a magnetic moment of $1.72\mu_B$ per Co atom), in good agreement with TEM observations.
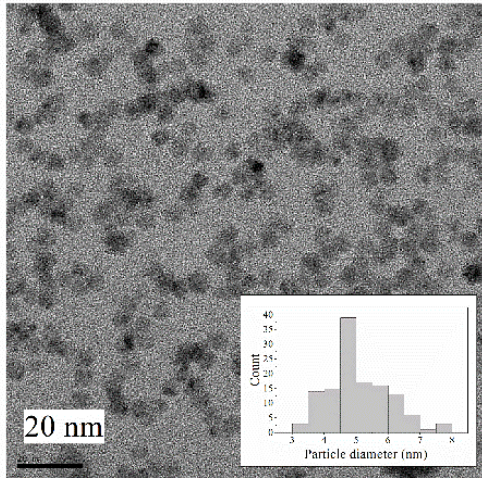
Figure 2. Representative TEM image of the Co nanoparticles. The scale bar at the bottom left corresponds to 20 nm. Shown in the inset is the corresponding particle size distribution.
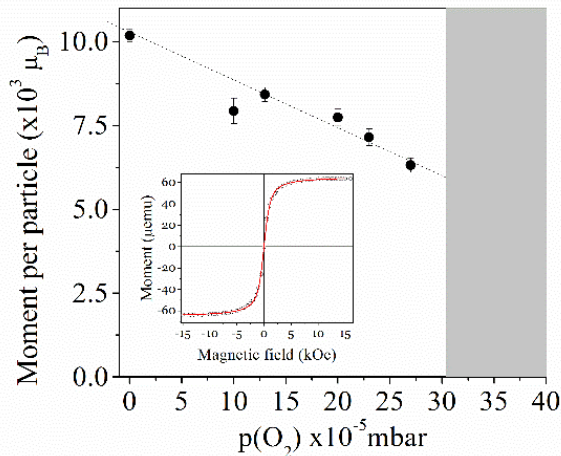

Figure 3. Evolution of the moment per particle on the O_2 pressure, as deduced from Langevin fits to room temperature loops, for the samples that could be satisfactorily fitted to such a Langevin function. Note that for high p_{O2} the loops show a weak secondary magnetic contribution, making it impossible to reliably fit then using Langevin function. The inset shows the 300K loop of the reference sample grown with no O_2 in the chamber, together with its fit (red line).

Note that the conditions for the nanoparticle generation in the cluster source are the same for all the samples. Consequently, the number of particles in each sample should be roughly the same for all samples. Thus, any changes in the saturation moment [Fig. 4(d)] of the samples should primarily arise from the partial oxidation of the Co nanoparticles. As can be seen in Fig. 4, the values of both H_E and H_C at 10 K exhibit an analogous non–monotonic behavior with p_{O2}, with maxima at around $p_{O2} = 23 \cdot 10^{-5}$ mbar. Interestingly, the maximum values of H_E and H_C (7780 and 6850 Oe, respectively) are extraordinarily large for a Co/CoO diluted system with very thin CoO shells (t_{CoO}=0.4–0.6 nm) and approach values typical of very dense systems (with strong shell–shell interactions)[32] or Co/CoO nanoparticles embedded in a CoO matrix.[31,36] Since the nanoparticles are grown as pure Co clusters and develop CoO shells during flight through the O2 atmosphere towards the substrate, the shell thickness (and thus the core diameter) could vary with p_{O2}. These changes could affect the evolution of the exchange bias properties with p_{O2}. A Langevin fit to the high temperature hysteresis loop of the different samples shows that, indeed, the average particle magnetic moment, and consequently the core diameter, decreases monotonically with increasing p_{O2} (see Fig. 3). Hence, as p_{O2} becomes higher the core diameter decreases, while the shell thickness concomitantly increases. However, a simple calculation shows that the changes are not significant: the core diameter is reduced from 5.0 nm to 4.2 nm, leading to a shell thickness increase of merely 0.6 nm (taking into account the lower density of CoO with respect to Co). Since the radius of the core (equivalent to the thickness of the ferromagnet in the well–known formula for thin films $\mu_0 H_E = \gamma/M_{FM}t_{FM}$)[1,2] becomes smaller as p_{O2} increases, H_E is expected to increase monotonically due to the $H_E \propto 1/t_{FM}$ relationship. Moreover, it is well–known that when the AFM thickness is very small virtually no bias is induced.[27,56] As the AFM thickness increases slightly, H_E should also monotonically increase,[27,56] as observed for small p_{O2}. Notably, in some systems, in particular in thin films, for thick enough AFM layers H_E can eventually decrease.[56] In fact, similar effects have been observed in Co/CoO nanoparticles.[57] However, the H_E reduction with AFM thickness occurs for much thicker AFM layers than the shells formed in our nanoparticles.[56,57] Hence, although the slight changes in morphology of the Co/CoO samples with p_{O2} may explain the increase in H_E and H_C for small p_{O2}, the decrease in H_E for high O2 contents must have some other origin.

Since the matrix has been shown to play an important role in the magnetism of Co/CoO nanoparticles, we next evaluate the evolution of the matrix with p_{O2}. The matrices may contain different proportions of the different possible Cu_xO phases: Cu, Cu_2O, Cu_4O_3 and CuO. From this list two interesting cases should be highlighted: (i) Cu_2O which has a very good lattice match to CoO (with only ~0.3% mismatch) and thus could lead to a "structural stabilization" (i.e., a higher degree of crystalline order) of CoO resulting in improved antiferromagnetic properties,[32] and (ii) CuO which is antiferromagnetic with a Néel temperature of $T_N = 200$ K and thus could enhance the magnetic properties due to exchange coupling.[36]
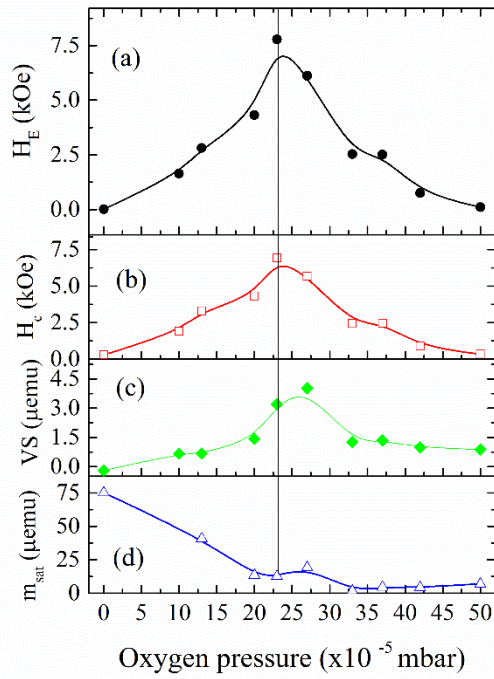
Figure 4. Dependence at T=10K of the (a) exchange bias, H_E, (b) coercivity, H_C, (c) vertical shift and (d) saturation moment of all the samples studied on the oxygen pressure, p_{O2}. The lines are guides to the eye.

As can be seen in Fig. 5, quantitative phase analysis (via the Rietveld method) of the XRD patterns shows that, with increasing p_{O2}, there is certainly an evolution of the phases present in the matrix towards more oxidized states of Cu. Remarkably, the main improvement of the exchange bias properties occurs as the Cu_2O phase appears, while the worsening of the properties for large p_{O2} is linked to the presence of CuO. However, an exact matching between the maximum H_E and the amount of Cu_2O is not observed probably because of the presence of Cu_4O_3 around the optimal pressure p_{O2}=23·10^{-5} mbar. Although Cu_4O_3 (AFM with T_N = 40 K)[58] could play a role, it is likely that the evolution of the lattice parameter of Cu_2O (and for example the presence of microstrains) with p_{O2} could be the dominating factor. Other factors, such as the increase in shell thickness and decrease in core diameter, will be simultaneously influencing the magnetic properties, thus one–to–one correlations between structure and magnetism are somewhat difficult. In any case, our results unambiguously show that for Co/CoO nanoparticles, the structural–stabilization of the shell is the dominant factor enhancing the magnetic properties, with exchange–stabilization playing a secondary role.

Another outstanding aspect of our results is the unexpectedly large H_E and H_C values observed in optimal p_{O2} conditions. The current understanding of exchange bias is based on the existence of uncompensated spins. Two types of uncompensated spins have been identified: pinned (unaffected by the magnetic field and which give rise to H_E) and unpinned or rotatable (which are dragged by the FM component and are related to the enhancement of H_C).[59–63]
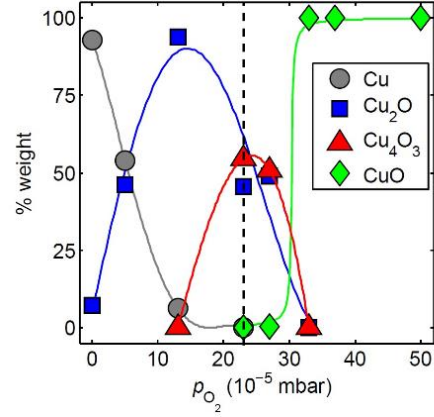

Figure 5. Evolution of the crystalline composition of the matrix on p_{O2}. The solid lines are guides to the eye. The vertical dashed line indicates the pressure at which a maximum in the exchange-bias field is observed.

In a hysteresis loop the pinned uncompensated spins are evidenced by a vertical shift.[50] Assuming that, once the FM magnetization is switched, the rotatable uncompensated spins can be further dragged by the applied magnetic field, then χ_{HF} should have a contribution from these uncompensated spins.[52–55] From panel (c) of Fig. 4, it is clear that the behavior of the pinned uncompensated spins (as quantified by the vertical shift) is similar to that displayed by H_E. Similarly, the dependence of χ_{HF} on p_{O2} (Fig. S2), which should carry out information about the rotatable uncompensated spins (see Supporting Information), resembles that of H_C. Interestingly, in thin films it has been shown that the dilution of the magnetic ions in the AFM layers by similar non–magnetic ions leads to a marked increase in H_E and H_C (e.g., CoO–Mg, FeMn–Cu, FeF_2–Zn).[29,64–66] Hence, in analogy to thin film systems, the large increase of H_E and H_C in the Co/CoO samples is due to the large increase in the number of uncompensated (pinned and unpinned) spins for intermediate O_2 pressures, presumably linked to a "dilution effect" in the CoO shell. Such effect is probably brought about by intermixing between the CoO shell and the Cu atoms of the Cu_xO matrix during the particle–matrix co–deposition,[36,67] which is undoubtedly enhanced by the lattice matching effect between Cu_2O and CoO.

To rule out any effect related to the small morphological changes caused by the O_2 in the chamber (core diameter - shell thickness) and to confirm the dominating role of the matrix in the observed effects, we have fabricated a second series of samples with Ag as matrix, instead of Cu, while keeping all conditions unaffected (see Supporting Information, SI). Note that, although both Ag and Ag_2O have a cubic structure, the lattice matching with CoO is considerably worse than for Cu_2O (Ag – mismatch 4.2%; Ag_2O – mismatch 10.6%). As can be seen in Fig. S1, the Ag_xO-matrix series also shows a maximum with p_{O2}. However, compared to the Cu_xO-matrix (Fig. S2) (i) the maximum occurs at much lower p_{O2}, (ii) the H_E values are remarkably smaller, and (iii) both the vertical shift and χ_{HF} are much smaller and without a clear link to H_E. These results eliminate the possibility that the small p_{O2}-induced morphological changes contribute significantly to the enhanced exchange bias properties. Interestingly, as expected, the maximum in H_E occurs at rather low p_{O2}, in the region where the Ag-based cubic phases exist; between the pure Ag

matrix and the Ag_2O dominated matrix.[68,69] The fact that the maximum H_E does not coincide with the best matched matrix (i.e., pure Ag) is probably due to the competition between the better lattice matching of the Ag matrix (which would better structurally stabilize the thin CoO shell) and the oxide character of the Ag_2O matrix. Namely, although Ag has a better lattice matching, the fact that it is not an oxide probably makes it more difficult for the Ag to diffuse into the CoO shell. A combination of poor matching (hence, low structural stabilization) and the limited interdiffusion (i.e., fewer uncompensated spins) is understood to be the origin of the greatly reduced H_E in the Ag_xO-matrix when compared to the Cu_xO-matrix. Moreover, it should be taken into account that when growing without O_2 the CoO shell probably would be very thin (only due to the residual O_2 in the chamber), which could also lead to reduced H_E in the $p_{O2} = 0$ case. Nevertheless, it is worth emphasizing that although the maximum H_E values for the Ag_xO-matrix ($H_E = 300$ Oe) are smaller than for the Cu_xO-matrix, given the cubic character of the Ag_xO-matrix for low p_{O2} (and thus a moderate lattice matching), these values are much larger than for matrices with no structural matching, e.g., Al_2O_3 which exhibit H_E values of only a few Oe.[32]

Further evidence of the enhanced properties for the lattice–matched samples arises from the temperature dependence of H_E. As can be seen in Fig. 6, the samples with optimal O_2 pressure exhibit an exchange bias blocking temperature $T_B^{H_E}$ (i.e., T at which H_E vanishes) of about 200 K. This value is typical of high quality isolated Co/CoO nanoparticles with substantially thicker CoO shells than in the NPs discussed here.[42] On the other hand, as the O_2 pressure varies away from the optimum value, $T_B^{H_E}$ quickly decreases, as shown for the $p_{O2} = 13 \cdot 10^{-5}$ and $50 \cdot 10^{-5}$ mbar samples in Fig. 6. In fact, the dependence of $T_B^{H_E}$ on p_{O2} nicely mimics the dependence of $H_E(p_{O2})$ (compare the inset of Fig. 6 with Fig. 4 (a)). These results indicate that the optimum p_{O2} not only enhances H_E but it stabilizes the exchange bias of the nanoparticles. This is in contrast to what has been observed for thin films where often an increase of H_E is usually accompanied by a decrease in $T_B^{H_E}$ [29,64–66] and thus gives further credibility to the structural stabilization model, since it shows that despite the magnetic dilution behind the enhanced H_E (which is the origin of the decreased $T_B^{H_E}$ in thin films), is actually highest for the samples with the largest H_E. $T_B^{H_E}$ is understood to be linked to the magnetic anisotropy energy of the CoO shell, i.e., $T_B^{H_E} \propto K_{CoO}V_{CoO}$ (where K and V are the anisotropy and the volume of the CoO grains, respectively). If we assume that V_{CoO} does not change considerably between samples, an increase in $T_B^{H_E}$ should imply a higher K_{CoO}, which would be expected for shells with a high degree of crystalline order. Additionally, the $T_B^{H_E}$ data allows us to rule out any leading role of exchange coupling in the enhanced properties, since for the case of $p_{O2}=23 \cdot 10^{-5}$ mbar no anomaly is seen about the Néel temperature of Cu_3O_4 [$T_N(Cu_3O_4)= 40$ K]. Similarly, for high p_{O2}, where the CuO matrix is dominant, $T_B^{H_E}$ is clearly below $T_N(CuO) = 200$ K, in contrast to when a NiO matrix is used (where exchange coupling is known to be dominant).[36]
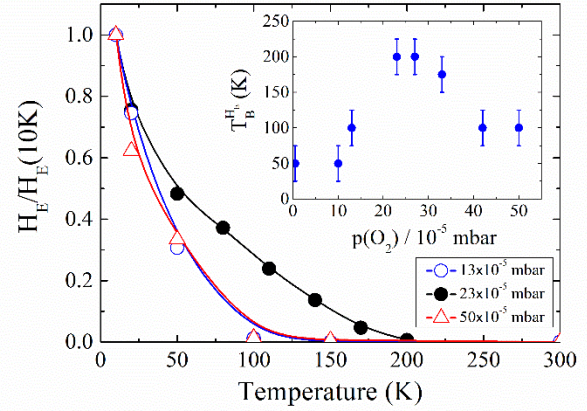

Figure 6. Temperature dependence of the normalized H_E, $H_E(T)/H_E(10$ K). Shown in the inset is the dependence of exchange bias blocking temperature, $T_B^{H_E}$, on the oxygen pressure, $p(O_2)$ The lines are guides to the eye.

CONCLUSIONS

In summary, we have studied the exchange bias properties of Co/CoO core/shell nanoparticles embedded in different Cu_xO matrices. The results show that H_E, H_C and $T_B^{H_E}$ are enhanced when the matrix is partially formed by Cu_2O, which has a good lattice parameter match with that of the CoO shell. In fact, for the optimized conditions both H_E and H_C present very large values (7780 and 6950 Oe, respectively), which can be linked to the presence of a large number of uncompensated spins (pinned and unpinned) in the CoO shell, induced by interdiffusion of Cu ions from the matrix to the shell during the sputtering. The results highlight the importance of the surrounding matrix to improve the crystalline quality of the thin CoO shells in the Co/CoO nanoparticles. Hence we demonstrate that lattice matching may be a highly efficient strategy to improve the magnetic properties of certain core/shell nanoparticle systems.

AUTHOR INFORMATION

Corresponding Author

* Email: j.a.gonzalez@uclm.es

ACKNOWLEDGMENT

REFERENCES

(1)   Nogués, J.; Sort, J.; Langlais, V.; Skumryev, V.; Suriñach, S.; Muñoz, J. S.; Baró, M. D. Exchange Bias in Nanostructures. *Phys. Rep.* **2005**, *422* (3), 65–117.

(2)   Nogués, J.; Schuller, I. K. Exchange Bias. *J. Magn. Magn. Mater.* **1999**, *192* (2), 203–232.

(3)   Vasilakaki, M.; Trohidou, K. N.; Nogués, J. Enhanced Magnetic Properties in Antiferromagnetic-Core/Ferrimagnetic-Shell Nanoparticles. *Sci. Rep.* **2015**, *5*, 9609.

(4)   O 'grady, K.; Fernández-Outon, L. E.; Vallejo-Fernández, G. A

New Paradigm for Exchange Bias in Polycrystalline Thin Films. *J. Magn. Magn. Mater.* **2009**, *322*, 883–899.

(5) Iglesias, O.; Labarta, A. A.; Batlle, X. Exchange Bias Phenomenology and Models of Core/shell Nanoparticles. *J. Nanosci. Nanotechnol.* **2008**, *8* (6), 2761–2780.

(6) Parkin, S.; Jiang, X.; Kaiser, C.; Panchula, A.; Roche, K.; Samant, M. Magnetically Engineered Spintronic Sensors and Memory. *Proc. IEEE* **2003**, *91* (5), 661–679.

(7) Leitao, D. C.; Silva, A. V; Paz, E.; Ferreira, R.; Cardoso, S.; Freitas, P. P. Magnetoresistive Nanosensors: Controlling Magnetism at the Nanoscale. *Nanotechnology* **2016**, *27* (4), 45501.

(8) Zhang, W.; Krishnan, K. M. Epitaxial Exchange-Bias Systems: From Fundamentals to Future Spin-Orbitronics. *Mater. Sci. Eng. R* **2016**, *105*, 1–20.

(9) Sort, J.; Suriñach, S.; Muñoz, J. S.; Baró, M. D.; Nogués, J.; Chouteau, G.; Skumryev, V.; Hadjipanayis, G. C. Improving the Energy Product of Hard Magnetic Materials. *Phys. Rev. B* **2002**, *65* (17), 174420.

(10) Lottini, E.; López-Ortega, A.; Bertoni, G.; Turner, S.; Meledina, M.; Van Tendeloo, G.; de Julián Fernández, C.; Sangregorio, C. Strongly Exchange Coupled Core/shell Nanoparticles with High Magnetic Anisotropy a Novel Strategy towards RE-Free Permanent Magnets. *Chem. Mater.* **2016**, *28* (12), 4214–4222.

(11) Wang, Z.; Bi, H.; Wang, P.; Wang, M.; Liu, Z.; Shen, L.; Liu, X. Magnetic and Microwave Absorption Properties of Self-Assemblies Composed of Core–shell Cobalt–cobalt Oxide Nanocrystals. *Phys. Chem. Chem. Phys.* **2014**, *17* (5), 3796–3801.

(12) Yusuf, S. M.; Manna, P. K.; Shirolkar, M. M.; Kulkarni, S. K.; Tewari, R.; Dey, G. K. A Study of Exchange Bias in BiFeO3 core/NiFe2O4 Shell Nanoparticles. *J. Appl. Phys.* **2013**, *113* (17), 173906.

(13) Groza, I.; Morel, R.; Brenac, A.; Beigné, C.; Notin, L. Electrical and Magnetic Properties of Co / CoO Core-Shell Clusters. *IEEE Trans. Magn.* **2011**, *47* (10), 3355–3357.

(14) Nayak, A. K.; Nicklas, M.; Chadov, S.; Khuntia, P.; Shekhar, C.; Kalache, A.; Baenitz, M.; Skourski, Y.; Guduru, V. K.; Puri, A.; Zeitler, U.; Coey, J. M. D.; Felser, C. Design of Compensated Ferrimagnetic Heusler Alloys for Giant Tunable Exchange Bias. *Nat. Mater.* **2015**, *14* (1), 679–684.

(15) McEnroe, S. a; Carter-Stiglitz, B.; Harrison, R. J.; Robinson, P.; Fabian, K.; McCammon, C. Magnetic Exchange Bias of More than 1 Tesla in a Natural Mineral Intergrowth. *Nat. Nanotechnol.* **2007**, *2* (10), 631–634.

(16) Jiménez-Villacorta, F.; Marion, J. L.; Sepehrifar, T.; Daniil, M.; Willard, M. A.; Lewis, L. H. Exchange Anisotropy in the Nanostructured MnAl System. *Appl. Phys. Lett.* **2012**, *100* (11), 112408.

(17) Jiménez-Villacorta, F.; Marion, J. L.; Sepehrifar, T.; Lewis, L. H. Tuning Exchange Anisotropy in Nanocomposite AgMn Alloys. *J. Appl. Phys.* **2012**, *111* (7), 07E141.

(18) Nayak, S.; Joshi, D. C.; Krautz, M.; Waske, A.; Eckert, J.; Thota, S. Reentrant Spin-Glass Behavior and Bipolar Exchange-Bias Effect in "Sn" Substituted Cobalt-Orthotitanate. *J. Appl. Phys.* **2016**, *119*, 43901.

(19) Chen, K.; Lott, D.; Radu, F.; Choueikani, F.; Otero, E.; Ohresser, P. Observation of an Atomic Exchange Bias Effect in DyCo 4 Film. *Sci. Rep.* **2015**, *5*, 18377.

(20) Harres, A.; Mikhov, M.; Skumryev, V.; Andrade, A. M. H. de; Schmidt, J. E.; Geshev, J. Criteria for Saturated Magnetization Loop. *J. Magn. Magn. Mater.* **2015**, *402*, 76–82.

(21) Salazar-Álvarez, G.; Sort, J.; Suriñach, S.; Baró, M. D.; Nogués, J. Synthesis and Size-Dependent Exchange Bias in Inverted Core-Shell MnO|Mn3O4 Nanoparticles. *J. Am. Chem. Soc.* **2007**, *129* (29), 9102–9108.

(22) Jungblut, R.; Coehoorn, R.; Johnson, M. T.; Aan De Stegge, J.; Reinders, A. Orientational Dependence of the Exchange Biasing in Molecular-Beam-Epitaxy- Grown Ni80Fe20/Fe50Mn50 Bilayers (Invited). *J. Appl. Phys.* **1994**, *75* (10), 6659–6664.

(23) Fitzsimmons, M.; Leighton, C.; Nogués, J.; Hoffmann, A.; Liu, K.; Majkrzak, C.; Dura, J.; Groves, J.; Springer, R.; Arendt, P.; Leiner, V.; Lauter, H.; Schuller, I. Influence of in-Plane Crystalline Quality of an Antiferromagnet on Perpendicular Exchange Coupling and Exchange Bias. *Phys. Rev. B* **2002**, *65*

(13), 134436.

(24) Lund, M.; Macedo, W.; Liu, K.; Nogués, J.; Schuller, I.; Leighton, C. Effect of Anisotropy on the Critical Antiferromagnet Thickness in Exchange-Biased Bilayers. *Phys. Rev. B* **2002**, *66* (5), 54422.

(25) Kuch, W.; Chelaru, L. I.; Offi, F.; Wang, J.; Kotsugi, M.; Kirschner, J. Tuning the Magnetic Coupling across Ultrathin Antiferromagnetic Films by Controlling Atomic-Scale Roughness. *Nat. Mater.* **2006**, *5* (2), 128–133.

(26) Fitzsimmons, M. R.; Lederman, D.; Cheon, M.; Shi, H.; Olamit, J.; Roshchin, I. V.; Schuller, I. K. Antiferromagnetic Domain Size and Exchange Bias. *Phys. Rev. B* **2008**, *77* (22), 224406.

(27) Schuller, I. K.; Morales, R.; Batlle, X.; Nowak, U.; Güntherodt, G. Role of the Antiferromagnetic Bulk Spins in Exchange Bias. *J. Magn. Magn. Mater.* **2016**, *416*, 2–9.

(28) Ali, M.; Marrows, C.; Hickey, B. Controlled Enhancement or Suppression of Exchange Biasing Using Impurity δ Layers. *Phys. Rev. B* **2008**, *77* (13), 134401.

(29) Miltényi, P.; Gierlings, M.; Keller, J.; Beschoten, B.; Güntherodt, G.; Nowak, U.; Usadel, K.; Miltenyi, P.; Gierlings, M.; Keller, J.; Beschoten, B.; Guntherodt, G.; Nowak, U.; Usadel, K. Diluted Antiferromagnets in Exchange Bias: Proof of the Domain State Model. *Phys. Rev. Lett.* **2000**, *84* (18), 4224–4227.

(30) Meiklejohn, W. H.; Bean, C. P. New Magnetic Anisotropy. *Phys. Rev.* **1956**, *102* (5), 1413–1414.

(31) Skumryev, V.; Stoyanov, S.; Zhang, Y.; Hadjipanayis, G.; Givord, D.; Nogués, J. Beating the Superparamagnetic Limit with Exchange Bias. *Nature* **2003**, *423* (6942), 850–853.

(32) Nogués, J.; Skumryev, V.; Sort, J.; Stoyanov, S.; Givord, D. Shell-Driven Magnetic Stability in Core-Shell Nanoparticles. *Phys. Rev. Lett.* **2006**, *97* (15), 157203.

(33) Ge, C.; Wan, X.; Pellegrin, E.; Hu, Z.; Manuel Valvidares, S.; Barla, A.; Liang, W.-I.; Chu, Y.-H.; Zou, W.; Du, Y. Direct Observation of Rotatable Uncompensated Spins in the Exchange Bias System Co/CoO-MgO. *Nanoscale* **2013**, *5* (21), 10236–10241.

(34) Feygenson, M.; Kou, A.; Kreno, L. E.; Tiano, A. L.; Patete, J. M.; Zhang, F.; Kim, M. S.; Solovyov, V.; Wong, S. S.; Aronson, M. C. Properties of Highly Crystalline NiO and Ni Nanoparticles Prepared by High-Temperature Oxidation and Reduction. *Phys. Rev. B* **2010**, *81* (1), 14420.

(35) González, J. A.; Andrés, J. P.; Toro, J. A.; Muñiz, P.; Muñoz, T.; Crisan, O.; Binns, C.; Riveiro, J. M. Co–CoO Nanoparticles Prepared by Reactive Gas-Phase Aggregation. *J. Nanoparticle Res* **2009**, *11* (8), 2105–2111.

(36) De Toro, J. A.; Marques, D. P.; Muñiz, P.; Skumryev, V.; Sort, J.; Givord, D.; Nogués, J. High Temperature Magnetic Stabilization of Cobalt Nanoparticles by an Antiferromagnetic Proximity Effect. *Phys. Rev. Lett.* **2015**, *115* (5), 57201.

(37) Tracy, J. B.; Weiss, D. N.; Dinega, D. P.; Bawendi, M. G. Exchange Biasing and Magnetic Properties of Partially and Fully Oxidized Colloidal Cobalt Nanoparticles. *Phys. Rev. B* **2005**, *72*, 64404.

(38) Tracy, J. B.; Bawendi, M. G. Defects in CoO in Oxidized Cobalt Nanoparticles Dominate Exchange Biasing and Exhibit Anomalous Magnetic Properties. *Phys. Rev. B* **2006**, *74*, 184434.

(39) Rinaldi-Montes, N.; Gorria, P.; Martínez-Blanco, D.; Amghouz, Z.; Fuertes, A. B.; Barquín, L. F.; Fernández, J. R.; Olivi, L.; Aquilanti, G.; Blanco, J. A. Disentangling Magnetic Core/shell Morphologies in Co-Based Nanoparticles. *J. Mater. Chem. C* **2016**, *4*, 2302–2311.

(40) Peng, D.; Sumiyama, K.; Hihara, T.; Yamamuro, S.; Konno, T. Magnetic Properties of Monodispersed Co/CoO Clusters. *Phys. Rev. B* **2000**, *61* (4), 3103–3109.

(41) Inderhees, S. E.; Borchers, J. A.; Green, K. S.; Kim, M. S.; Sun, K.; Strycker, G. L.; Aronson, M. C. Manipulating the Magnetic Structure of Co Core/CoO Shell Nanoparticles: Implications for Controlling the Exchange Bias. *Phys. Rev. Lett.* **2008**, *101* (11), 117202.

(42) De Toro, J. A.; Andrés, J. P.; González, J. A.; Riveiro, J. M.; Estrader, M.; López–Ortega, A.; Tsiaoussis, I.; Frangis, N.; Nogués, J. Role of the Oxygen Partial Pressure in the Formation of Composite Co-CoO Nanoparticles by Reactive Aggregation.

J. Nanoparticle Res. **2011**, *13* (10), 4583–4590.

(43) Margaris, G.; Trohidou, K. N.; Nogués, J. Mesoscopic Model for the Simulation of Large Arrays of Bi-Magnetic Core/shell Nanoparticles. *Adv. Mater.* **2012**, *24* (31), 4331–4336.

(44) Lavorato, G. C.; Lima, E.; Troiani, H. E.; Zysler, R. D.; Winkler, E. L. Exchange-Coupling in Thermal Annealed Bimagnetic Core/shell Nanoparticles. *J. Alloys Compd.* **2015**, *633*, 333–337.

(45) Wiedwald, U.; Spasova, M.; Salabas, E.; Ulmeanu, M.; Farle, M.; Frait, Z.; Rodriguez, A.; Arvanitis, D.; Sobal, N.; Hilgendorff, M.; Giersig, M. Ratio of Orbital-to-Spin Magnetic Moment in Co Core-Shell Nanoparticles. *Phys. Rev. B* **2003**, *68* (6), 64424.

(46) Portemont, C.; Morel, R.; Brenac, A.; Notin, L. Exchange Bias between Cobalt Clusters and Oxide Thin Films. *J. Appl. Phys.* **2006**, *100* (3), 33907.

(47) De Toro, J. A.; González, J. A.; Normile, P. S.; Muñiz, P.; Andrés, J.; López Antón, R.; Canales-Vázquez, J.; Riveiro, J. M. Energy Barrier Enhancement by Weak Magnetic Interactions in Co/Nb Granular Films Assembled by Inert Gas Condensation. *Phys. Rev. B* **2012**, *85* (5), 54429.

(48) De Toro, J. A.; Andrés, J. P.; González, J. A.; Muñiz, P.; Riveiro, J. M. The Oxidation of Metal-Capped Co Cluster Films under Ambient Conditions. *Nanotechnology* **2009**, *20* (8), 85710.

(49) Rodríguez-Carvajal, J. Recent Advances in Magnetic Structure Determination Neutron Powder Diffraction. *Phys. B* **1993**, *192*, 55–69.

(50) Nogués, J.; Leighton, C.; Schuller, I. Correlation between Antiferromagnetic Interface Coupling and Positive Exchange Bias. *Phys. Rev. B* **2000**, *61* (2), 1315–1317.

(51) Chikazumi, S. *Physics of Ferromagnetism*, 2nd ed.; Oxford University Press: New York, 1997.

(52) Khurshid, H.; Li, W.; Phan, M.-H.; Mukherjee, P.; Hadjipanayis, G. C.; Srikanth, H. Surface Spin Disorder and Exchange-Bias in Hollow Maghemite Nanoparticles. *Appl. Phys. Lett.* **2012**, *101* (2), 22403.

(53) Cabot, A.; Alivisatos, a.; Puntes, V.; Balcells, L.; Iglesias, Ò.; Labarta, A. Magnetic Domains and Surface Effects in Hollow Maghemite Nanoparticles. *Phys. Rev. B* **2009**, *79* (9), 94419.

(54) Mishra, S. R.; Dubenko, I.; Losby, J.; Ghosh, K.; Khan, M.; Ali, N. Anomalous Magnetic Properties of Mechanically Milled Cobalt Oxide Nanoparticles. *J. Nanosci. Nanotechnol.* **2005**, *5* (12), 2076–2081.

(55) Zhang, H.-T.; Chen, X.-H. Controlled Synthesis and Anomalous Magnetic Properties of Relatively Monodisperse CoO Nanocrystals. *Nanotechnology* **2005**, *16* (10), 2288.

(56) Ali, M.; Marrows, C.; Hickey, B. Onset of Exchange Bias in Ultrathin Antiferromagnetic Layers. *Phys. Rev. B* **2003**, *67* (17), 172405.

(57) Feygenson, M.; Yiu, Y.; Kou, A.; Kim, K.-S.; Aronson, M. C.

(58) Pinsard-Gaudart, L.; Rodríguez-Carvajal, J.; Gukasov, A.; Monod, P. Magnetic Properties of Paramelaconite (Cu4O3): A Pyrochlore Lattice with S=1/2. *Phys. Rev. B* **2004**, *69* (10), 104408.

(59) Ohldag, H.; Scholl, A.; Nolting, F.; Arenholz, E.; Maat, S.; Young, A. T.; Carey, M.; Stöhr, J. Correlation between Exchange Bias and Pinned Interfacial Spins. *Phys. Rev. Lett.* **2003**, *91* (1), 17203.

(60) Camarero, J.; Pennec, Y.; Vogel, J.; Pizzini, S.; Cartier, M.; Fettar, F.; Ernult, F.; Tagliaferri, A.; Brookes, N.; Dieny, B. Field Dependent Exchange Coupling in NiO/Co Bilayers. *Phys. Rev. B* **2003**, *67*, 20413.

(61) Brück, S.; Schütz, G.; Goering, E.; Ji, X.; Krishnan, K. M. Uncompensated Moments in the MnPd/Fe Exchange Bias System. *Phys. Rev. Lett.* **2008**, *101* (12), 126402.

(62) Fitzsimmons, M. R.; Kirby, B. J.; Roy, S.; Li, Z.-P. P.; Roshchin, I. V.; Sinha, S. K.; Schuller, I. K. Pinned Magnetization in the Antiferromagnet and Ferromagnet of an Exchange Bias System. *Phys. Rev. B* **2007**, *75* (21), 214412.

(63) Gilbert, D. A.; Ye, L.; Varea, A.; Agramunt-Puig, S.; del Valle, N.; Navau, C.; López-Barbera, J. F.; Buchanan, K. S.; Hoffmann, A.; Sánchez, A.; Sort, J.; Liu, K.; Nogués, J. A New Reversal Mode in Exchange Coupled Antiferromagnetic/ferromagnetic Disks: Distorted Viscous Vortex. *Nanoscale* **2015**, *7* (21), 9878–9885.

(64) Fecioru-Morariu, M.; Ali, S. R.; Papusoi, C.; Sperlich, M.; Güntherodt, G. Effects of Cu Dilution in IrMn on the Exchange Bias of CoFe/IrMn Bilayers. *Phys. Rev. Lett.* **2007**, *99* (9), 97206.

(65) Shi, H.; Lederman, D.; Fullerton, E. E. Exchange Bias in Fe xZn 1-xF 2/Co Bilayers. *J. Appl. Phys.* **2002**, *91*, 7763–7765.

(66) Hong, J. Il; Leo, T.; Smith, D. J.; Berkowitz, A. E. Enhancing Exchange Bias with Diluted Antiferromagnets. *Phys. Rev. Lett.* **2006**, *96* (11), 117204.

(67) Borchers, J. A.; Carey, M. J.; Erwin, R. W.; Majkrzak, C. F.; Berkowitz, A. E. Spatially Modulated Antiferromagnetic Order in CoO/NiO Superlattices. *Phys. Rev. Lett.* **1993**, *70* (12), 1878–1881.

(68) Riveiro, J. M.; Normile, P. S.; Andrés, J. P.; González, J. A.; De Toro, J. A.; Muñoz, T.; Muñiz, P. Oxygen-Assisted Control of Surface Morphology in Nonepitaxial Sputter Growth of Ag. *Appl. Phys. Lett.* **2006**, *89* (20), 201902.

(69) Reddy, P. N.; Sreedhar, A.; Reddy, M. H. P.; Uthanna, S.; Pierson, J. F. The Effect of Oxygen Partial Pressure on Physical Properties of Nano-Crystalline Silver Oxide Thin Films Deposited by RF Magnetron Sputtering. **2011**, *966* (9), 961–966.